



# CHORUS

This is the accepted manuscript made available via CHORUS. The article has been published as:

## Spin diffusion length and spin Hall angle in $\text{Pd}_{1-x}\text{Pt}_x/\text{YIG}$ heterostructures: Examination of spin relaxation mechanism

Li Ma, Lili Lang, Jeongwoo Kim, Zhe Yuan, Ruqian Wu, Shiming Zhou, and Xuepeng Qiu

Phys. Rev. B **98**, 224424 — Published 26 December 2018

DOI: [10.1103/PhysRevB.98.224424](https://doi.org/10.1103/PhysRevB.98.224424)

# Spin diffusion length and spin Hall angle in $\text{Pd}_{1-x}\text{Pt}_x/\text{YIG}$ heterostructures: Examination of spin relaxation mechanism

Li Ma<sup>1,4</sup>, Lili Lang<sup>1</sup>, Jeongwoo Kim<sup>2</sup>, Zhe Yuan<sup>3</sup>,  
Ruqian Wu<sup>2</sup>, Shiming Zhou<sup>1</sup> and Xuepeng Qiu<sup>1,\*</sup>

<sup>1</sup>*Shanghai Key Laboratory of Special Artificial Microstructure Materials and Technology and Pohl Institute of Solid State Physics and School of Physics Science and Engineering, Tongji University, Shanghai 200092, China*

<sup>2</sup>*Department of Physics and Astronomy, University of California, Irvine, California 92697-4575, USA*

<sup>3</sup>*The Center for Advanced Quantum Studies and Department of Physics, Beijing Normal University, 100875 Beijing, China*

<sup>4</sup>*School of Materials Science and Engineering, Xi'an University of Technology, Xi'an 710048, China*

## Abstract

The thickness, temperature and composition studies of spin diffusion length (SDL) and spin Hall angle (SHA) are performed by measuring the spin Hall magnetoresistance in  $\text{Pd}_{1-x}\text{Pt}_x/\text{Y}_3\text{Fe}_5\text{O}_{12}$  (=YIG) heterostructures. The SDL is found to be invariant to changes in the electron momentum relaxation time by varying the temperature, the NM thickness, or the alloy composition, while the SHA exhibits a non-monotonic dependence on temperature. These findings suggest the appearance of D'yakonov-Perel' spin relaxation mechanism and phonon skew scattering in our heterostructures that is associated with strong interfacial Rashba spin orbit coupling (IRSOC). At last, we employ the *ab initio* calculations to quantify the IRSOC at the inversion symmetry broken NM/YIG interface.

## Introduction

In normal metal (NM)/ferromagnet (FM) heterostructures, spin orbit coupling (SOC) effect leads to interconversion between the charge and spin currents and drives many exotic phenomena, spin orbit torque<sup>1-3</sup>, Dzyaloshinskii-Moriya interaction<sup>4</sup>, terahertz emission<sup>5</sup>, spin Hall magnetoresistance<sup>6</sup>, *etc.* The charge to spin current interconversion is usually described by two material parameters, namely, spin Hall angle (SHA) and spin diffusion length (SDL). The SHA determines the conversion efficiency between charge and spin currents, while the parameter SDL gives the length scale over which the non-equilibrium spins can maintain their spin state and is closely correlated with the spin relaxation process<sup>7-9</sup>. It is noted that the SDL is also an essential precondition for the understanding of the SHA because they are entangled in experiments of the charge-spin current conversion<sup>6,10-14</sup>. Although the SDL in NM/FM heterostructures has been studied extensively in both experiments and theory<sup>15-19</sup>, results are still controversial. The measured values for Pt/FM heterostructures spread in a large range<sup>7-9</sup>. Moreover, different temperature (T) dependencies of SDL in Pt/Y<sub>3</sub>Fe<sub>5</sub>O<sub>12</sub>(YIG) have been reported<sup>18,19</sup>. The puzzle in the SDL is caused by intricate mechanisms of spin relaxation process, e.g., the Elliott-Yafet (E-Y) mechanism or/and the D'yakonov-Perel' (D-P) mechanism<sup>17,18,20-23</sup>.

In the E-Y mechanism for bulk materials with inversion symmetry<sup>24-26</sup>, the spin flip occurs after subsequent impurity scatterings which is schematically shown in Fig. 1(a). The spin relaxation time  $\tau_{s,EY}$  reads the following equation

$$\frac{1}{\tau_{s,EY}} \approx \frac{\alpha}{\tau_e}, \quad (1)$$

where  $\tau_e$  is the relaxation time of electron momentum in bulk materials, and the parameter  $\alpha$  is proportional to  $\xi^2$  with the bulk SOC strength  $\xi$  in the perturbation theory<sup>7,8,24-27</sup>.

The D-P mechanism of the spin relaxation process may play a non-negligible role in NM/FM heterostructures because of the broken inversion symmetry at interfaces<sup>27-29</sup>. Although the charge potential is screened at the NM surface (within Thomas-Fermi screening length), the interfacial asymmetry still can actively influence the metal interior within the electron phase relaxation length<sup>21,22,30,31</sup>. In D-P spin relaxation, the spin coherence is lost between successive scattering events due to the spin precession, as schematically shown in Fig. 1(b), and the spin

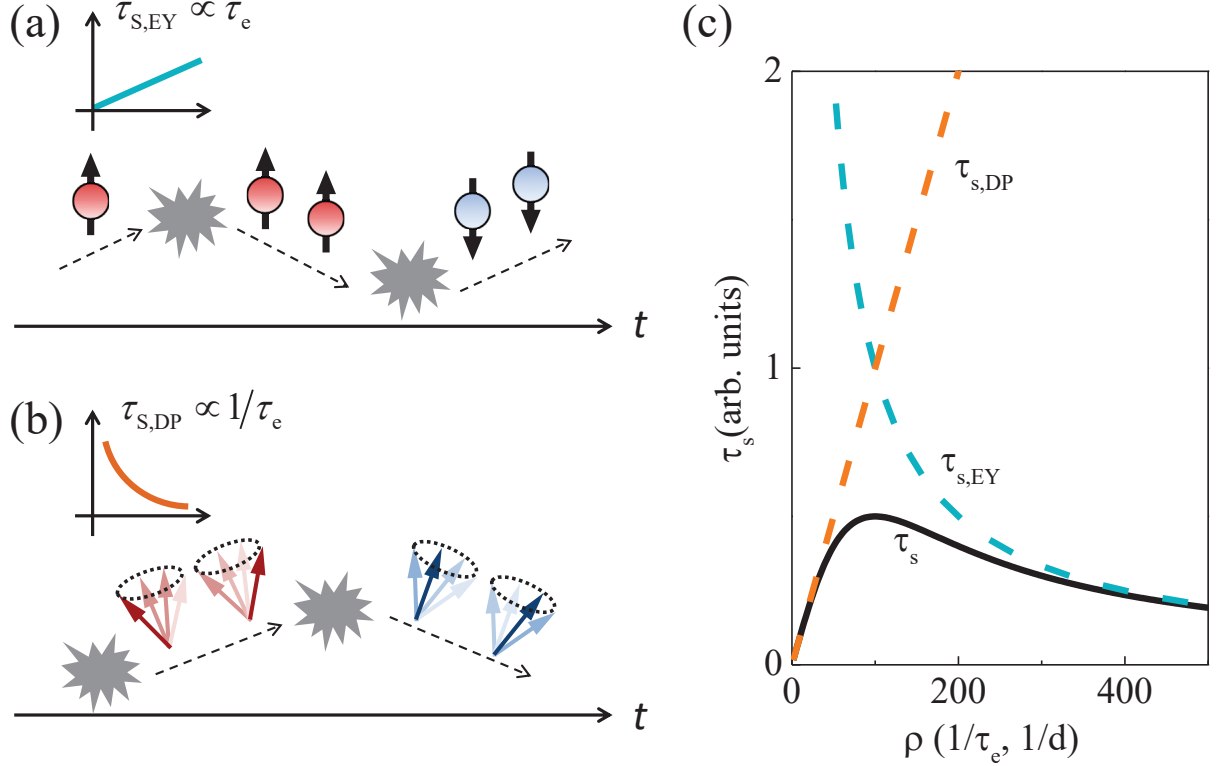


FIG. 1: Schematics of the spin relaxation processes in the E-Y<sup>24–26</sup> (a) and the D-P (b) models<sup>28,29</sup>. (c) The correlation between the entire spin relaxation time  $\tau_s$  and the sheet resistivity  $\rho$  ( $1/d$ ,  $1/\tau_e$ ). The D-P and the E-Y contributions, drawn as  $\tau_{s,DP}$  and  $\tau_{s,EY}$ , are also shown. Here,  $d$  and  $\tau_e$  are the NM layer thickness and the relaxation time of electron momentum, respectively.

relaxation time is given by the following equation

$$\frac{1}{\tau_{s,DP}} = \tau_e \langle \Omega_k^2 \rangle, \quad (2)$$

where the electron wave-vector dependent Larmor frequency  $\langle \Omega_k^2 \rangle \propto \xi_R^2$ , with  $\xi_R$  being the interfacial Rashba SOC (IRSOC) strength. The prerequisite for Eq. 2 is  $\tau_e \Omega_k \ll 1.0$ . The Rashba Hamiltonian is defined in the equation  $H_R = \xi_R (\vec{z} \times \vec{p}) \cdot \vec{\sigma}$  with the electron momentum  $\vec{p}$  and the vector of Pauli spin matrices  $\vec{\sigma}$ <sup>7,8,32</sup>. In general, the entire spin scattering rate in NM/FM heterostructures can be described by the following equation,  $\frac{1}{\tau_s} = a_1 \rho + b_1 / \rho$ , where the first and the second terms refer to the E-Y and the D-P models, respectively. The

entire spin relaxation time  $\tau_s$  changes nonmonotonically with the sheet resistivity, as shown in Fig. 1(c), where the parameters  $a_1 = 0.01$  and  $b_1 = 100$ .

According to the theoretical model proposed by Valet and Fert<sup>33</sup>, one has the SDL  $\lambda_{sd} = \sqrt{D\tau_s}$ , where the electron diffusion coefficient  $D$  depends on the Fermi velocity  $v_F$  as  $D = \tau_e v_F^2$  and  $\tau_s$  is the entire spin relaxation time. Therefore, regardless the mechanism of the spin relaxation process, either the E-Y model, the D-P one, or both<sup>24,26</sup>, it is necessary to study the SDL as a function of both the relaxation time of electron momentum and the (bulk or/and interfacial) SOC. In this work, we study the SDL and SHA in  $\text{Pd}_{1-x}\text{Pt}_x$  (PdPt)(top)/insulating- $\text{Y}_3\text{Fe}_5\text{O}_{12}$  (YIG) heterostructures on [111]-oriented single crystalline  $\text{Gd}_3\text{Ga}_5\text{O}_{12}$  (GGG) substrates and provide adequate insight into the underlying spin relaxation mechanism.

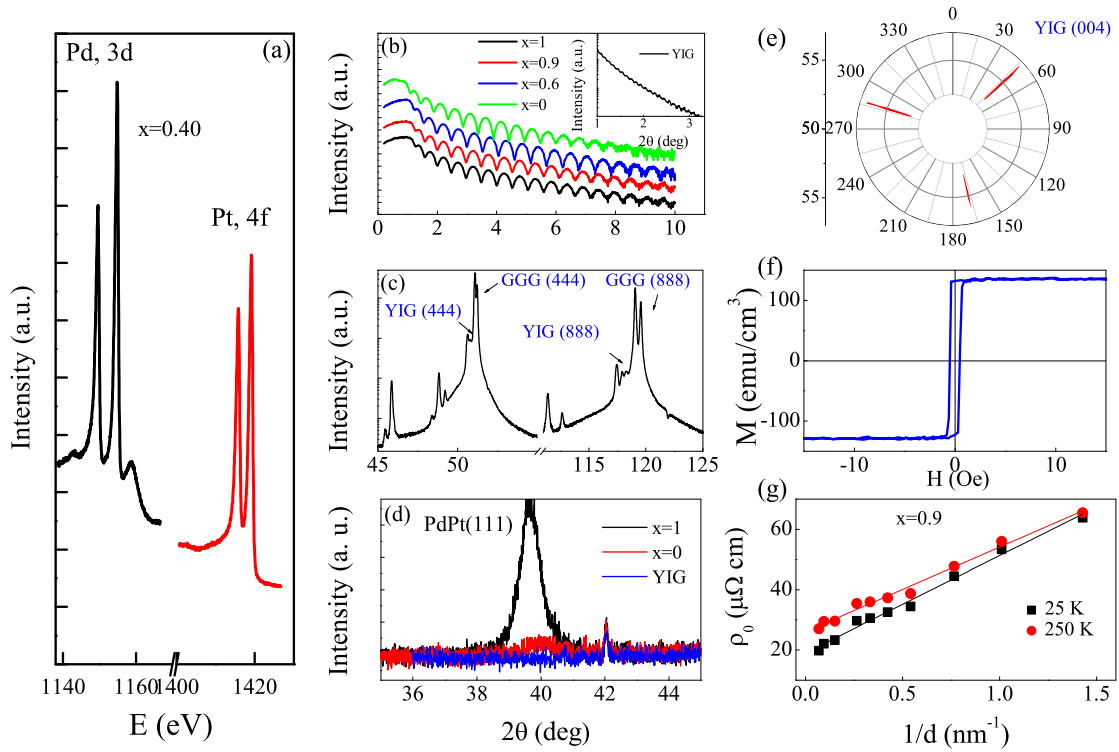


FIG. 2: Typical XPS results of  $\text{Pd}_{1-x}\text{Pt}_x$  with  $x = 0.40$  (a). Small angle XRR of 15 nm thick PdPt layer (b). Large angle XRD for 80 nm thick YIG film (c) and PdPt layer (d). For YIG film,  $\Phi$  and  $\Psi$  scans with a fixed  $2\theta$  for the (004) reflection (e) and magnetization hysteresis loop (f). The resistivity  $\rho_0$  versus  $1/d$  at 25 K and 250 K for  $\text{Pd}_{0.1}\text{Pt}_{0.9}/\text{YIG}$  heterostructure (g). In the inset of (b), small angle XRR of 80 nm thick YIG layer is shown.

## Experiments

80 nm thick single-crystal  $\text{Y}_3\text{Fe}_5\text{O}_{12}$  (YIG) films were grown on [111]-oriented single crystalline GGG substrates from a stoichiometric polycrystalline target via pulsed laser deposition (PLD). PdPt alloy layers were then deposited at ambient temperature on YIG thin films by DC magnetron sputtering in ultrahigh vacuum. The films were patterned into normal Hall bar and the longitudinal resistivity  $\rho_{xx}$  was measured by physical property measurement system (PPMS). The alloy composition of PdPt was measured by x-ray photoelectron spectroscopy (XPS, Kratos AXIS DLD). Typical results are shown in Fig. 2(a). The film thickness and microstructure were characterized by X-ray reflection (XRR) and X-ray diffraction (XRD), respectively, using a D8 Discover X-ray diffractometer with Cu  $K\alpha$  radiation. The XRR spectra in Fig. 2 (b) show that YIG and PdPt are  $80 \pm 2$  and  $15 \pm 1$  nm in thickness, respectively. Remarkably, the multi-oscillations and the lasting signal until very high  $2\theta$  in XRR spectra demonstrate the good surface roughness of the films of different composition. Figure 2(c) shows the XRD peaks at  $2\theta = 50.62$  and  $117.45$  degrees corresponding to (444) and (888) orientations in YIG films. PdPt layers are polycrystalline with [111] preferred orientation, as shown in Fig. 2(d). Epitaxial growth of the YIG on GGG was verified by  $\Phi$  and  $\Psi$  scans with  $2\theta$  fixed at 59.29 degrees for the (004) reflection of YIG film, as shown in Fig. 2(e). In-plane magnetization hysteresis loops were measured at room temperature via vibrating sample magnetometer, as shown in Fig. 2(f). The spontaneous magnetization is found to be  $136 \text{ emu/cm}^3$ , close to the theoretical value. The coercivity is as small as 1.0 Oe. Fig. 2(g) shows the linear scaled resistivity  $\rho_0$  with  $1/d$  for the  $x = 0.90$  sample at 25 K and 250 K, suggesting the continuity of the film for the studied thickness region.

## Results and discussion

Utilization of PdPt alloy allows the continuous tuning of IRSOC with the alloy composition<sup>34</sup>. Significantly, the relaxation time of electron momentum can be adjusted by changing the temperature, the NM layer thickness and, in particular, the alloy composition. The relaxation time of electron momentum reaches a minimum at the intermediate alloy composition. Spin Hall magnetoresistance (SMR), as a versatile approach to characterize the spin transport<sup>6</sup>, is employed to measure the SDL and the SHA. The longitudinal resistivity of the NM layer is

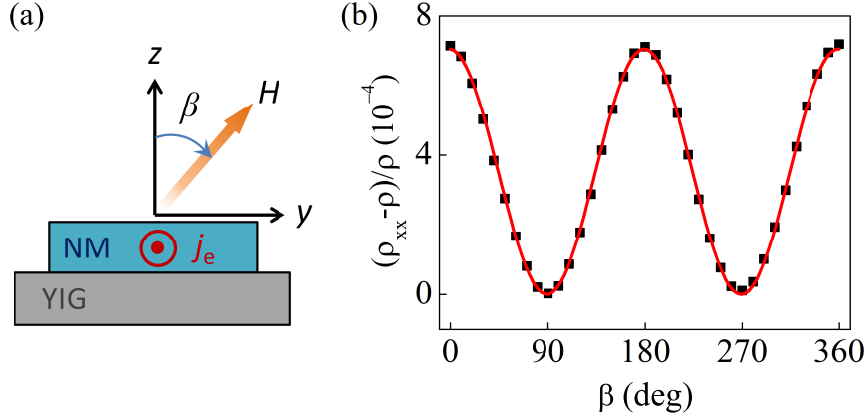


FIG. 3: SMR measurement (a) and typical angular dependent SMR in Pt(4 nm)/YIG(80 nm) (b). Here, the FM magnetization is almost saturated along the external magnetic field of 50.0 kOe. The solid line refers to the fitting according to the SMR theory<sup>6,13,14</sup>.

given as<sup>13,14</sup>

$$\rho_{xx} = \rho + \Delta\rho m_t^2, \quad (3)$$

where  $\rho$  refers to the longitudinal resistivity of NM/FM heterostructures at zero external magnetic field and the  $y$ -axis component of the magnetization unit vector  $m_t$  is perpendicular to the charge current, as shown in Fig. 3(a). As the external magnetic field rotates in the  $yz$  plane, the sheet resistivity  $\rho_{xx}$  obeys the Eq. 3, as shown in Fig. 3(b).

Figure 4 shows the SMR ratio of Pt/YIG and Pd<sub>0.60</sub>Pt<sub>0.40</sub>/YIG as a function of the NM layer thickness ( $d$ ) at various temperatures. For the two systems, the SMR ratio  $\Delta\rho/\rho$  at all temperatures changes non-monotonically with  $d$ , due to the decay of spin current density along the film normal direction. The magnitude of the SMR peak changes weakly at low temperatures and strongly at high temperatures for both Pt/YIG and PdPt/YIG. Moreover, the SMR in Pt/YIG is larger than that of PdPt/YIG. The observed results can be fitted by the following equation<sup>13</sup>

$$\Delta\rho/\rho = \theta_{SH}^2 \frac{\lambda_{sd}}{d} \frac{\tanh^2(d/2\lambda_{sd})}{1/2\rho\lambda_{sd}G_r + \coth(d/\lambda_{sd})}, \quad (4)$$

where the measured sheet resistivity  $\rho$  of the heterostructures at all temperatures changes as a linear function of  $1/d$ , as shown in Fig. 2(g). The real part of the spin mixing conductance  $G_r$  at the NM/FM interface is assumed to be independent of the NM layer thickness<sup>12</sup>. Here,  $G_r$  at room temperature was measured by spin pumping and ferromagnetic resonance techniques. The

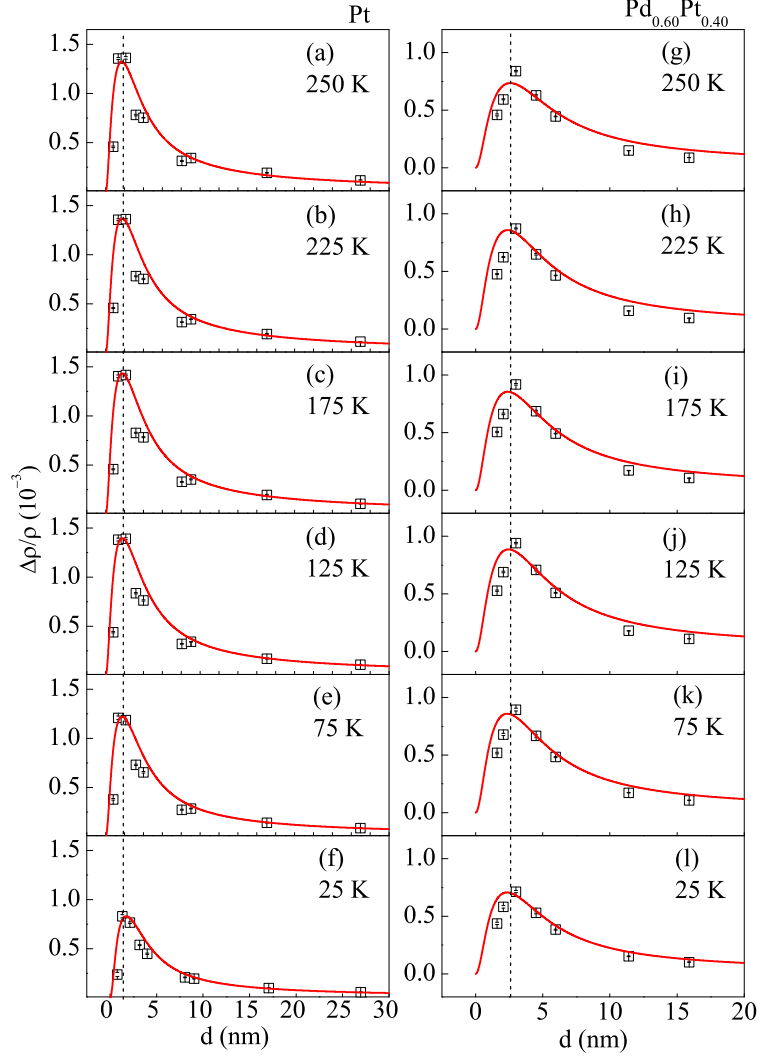


FIG. 4: SMR ratio of Pt/YIG (left column) and Pd<sub>0.60</sub>Pt<sub>0.40</sub>/YIG (right column) as a function of the NM layer thickness  $d$  at different temperatures. Solid lines represent the fitting results according to the SMR theory<sup>13</sup>, in combination of the D-P model. The SDL  $\lambda_{sd}$  at all temperatures is fitted to be  $1.15 \pm 0.02$  nm and  $1.56 \pm 0.02$  nm for Pt/YIG and Pd<sub>0.60</sub>Pt<sub>0.40</sub>/YIG, respectively. The inset numbers refer to measurement temperatures.

ferromagnetic resonance spectra of YIG and PdPt/YIG were measured at  $f = 9.0$  GHz, and then the resonance linewidth and thus the spin mixing conductance were obtained with Eq.4. Previous studies have shown that  $G_r$  below 300 K is approximately independent of temperature within experimental error<sup>12,19,35,36</sup>. Therefore, it is reasonable to assume the constant spin mixing conductance below room temperature and the value of  $G_r$  at low temperatures is taken as that of room temperature in the present work.

$$G_r = \frac{4\pi\gamma M_s t_{FM}}{g\mu_B\omega} (\Delta H_{NM/FM} - \Delta H_{FM}), \quad (5)$$

where  $t_{FM}$  and  $M_s$  are the FM layer thickness and the FM magnetization, respectively. The results of  $G_r$  as a function of the Pt atomic concentration are given in table I.

Pt atomic concentration $x =$	0	0.10	0.40	0.90	1.0
$G_r$ ( $10^{18}/m^2$ )	1.09	1.94	3.47	4.8	8.05

TABLE I: Spin mixing conductance of PdPt/YIG at room temperature<sup>37</sup>

Nonlinear least-square algorithms were employed to fit the measured thickness dependence of the SMR ratio for PdPt/YIG. The R-Square is used to reflect the degree of correlation between measured data and fitted data, as a key parameter in statistical mechanics. When the R-Square is in the region of 0.9-1.0, the fitting results are close to the experimental ones. Moreover, In order to disentangle the SHA and the SDL in Eq.4 for the SMR, the SHA  $\theta_{SH}$  is generally proved to be independent of the NM layer thickness in the fitting procedure<sup>12-14,36,38</sup>. A similar approach is adopted in the present work. Furthermore, at a specific temperature, the SMR results can be fitted by *a single value* of  $\lambda_{sd}$ , as shown in Fig. 4. The most remarkable observation is that, as marked by the vertical dash lines, the SMR peaks at different temperatures occur at the same  $d$  for both Pt and PdPt systems. As the position of the SMR peak is suggested to be determined by the ratio  $d/\lambda_{sd}$ <sup>19,39</sup>, it is indicated that  $\lambda_{sd}$  is also independent of temperature. Therefore, the SDL is independent of the relaxation time of electron momentum with varying temperature or  $d$ , in accordance with the D-P model. Finally,  $\lambda_{sd}$  at all temperatures is fitted to be  $1.15 \pm 0.02$  nm and  $1.56 \pm 0.02$  nm,  $3.55 \pm 0.32$  nm, and the SHA at 250 K is equal to 0.14, 0.098, and 0.061 for Pt/YIG, Pd<sub>0.60</sub>Pt<sub>0.40</sub>/YIG, and Pd/YIG systems, respectively.

For NM/FM heterostructures, the entire spin scattering rate can be generally described by the following equation<sup>22</sup>,  $\frac{1}{\tau_s} = \frac{\alpha}{\tau_e} + \langle \Omega_k^2 \rangle \tau_e$ , according to Eqs. 1 and 2, where the parameters  $\alpha$  and  $\langle \Omega_k^2 \rangle$  depend on the strengths of the bulk SOC and the IRSOC, respectively. In order to gain insight into the spin relaxation mechanism, the measured SMR results of Pt/YIG and Pd/YIG are fitted by considering the different fractal contributions of D-P and E-Y models to the SDL. As shown in Fig. 5, for either Pt/YIG or Pd/YIG, the SMR in the large  $d$  region

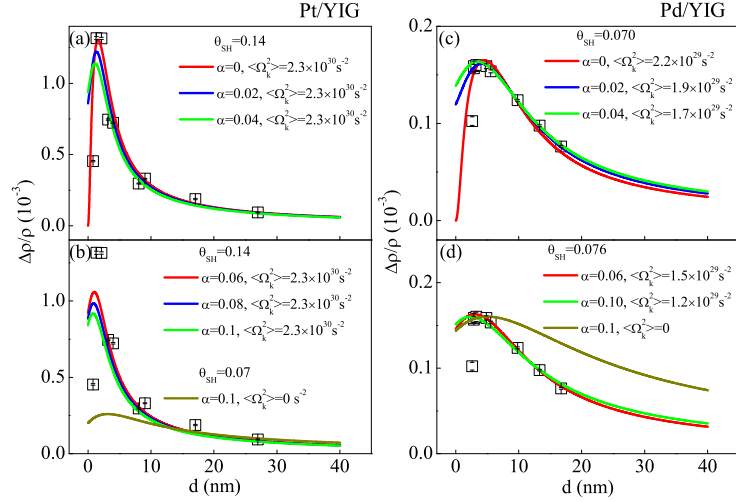


FIG. 5: Measured SMR (black, open boxes) and fitted results (lines) for Pt/YIG (a,b) and Pd/YIG (c,d) at 250 K. The values of the spin mixing conductance  $G_r$  in table I are used.

can be well fitted with different combinations of  $\alpha$  and  $\Omega_k$ . However, in the small  $d$  region, the experimental data can be better fitted by reducing the E-Y one and highlighting the fractal contribution from the D-P model. These results indicate that the D-P mechanism has an unnegligible contribution for the spin relaxation in NM/YIG heterostructures.

The calculations based on the D-P model, as shown in Fig. 6(a), reproduce well another major feature that the SMR peak does not shift with temperature, as shown in Fig. 4. Since  $\tau_s \propto 1/\tau_e$  in the D-P model and  $D \propto \tau_e$ ,  $\lambda_{sd}$  is independent of both  $d$  and  $T$ , as shown in Fig. 6(b), although  $\tau_e$  strongly depends on  $d$  and  $T$ . On the other hand, as  $\tau_s \propto \tau_e$  for the E-Y model<sup>24–26</sup>, the SMR peak would exhibit a shift with temperature, as shown in Fig. 6(c). The shift amplitude depends on both  $\sigma$  and  $\tau_e$  which in turn relies on the film quality. Since  $\lambda_{sd} \propto \tau_e$ ,  $\lambda_{sd}$  changes with both  $d$  and  $T$ , as shown in Fig. 6(d).

Figure 7 summarizes effects of the temperature, the NM layer thickness, and the Pt concentration on the spin relaxation time. In order to obtain the electron diffusion coefficient  $D$ , ordinary Hall effect of PdPt/YIG was measured, under the external magnetic field  $H$  perpendicular to the film plane. At high  $H$ , the Hall voltage  $V_H$  changes as a linear function of  $B$ . The Hall coefficient  $R_H$  can be calculated by the equation  $R_H = d \frac{dR_{xy}}{dB}$  with the NM layer thickness  $d$ , Hall resistance  $R_{xy} = V_H/I$  and sensing current  $I$ . Then, one has the Hall mobility

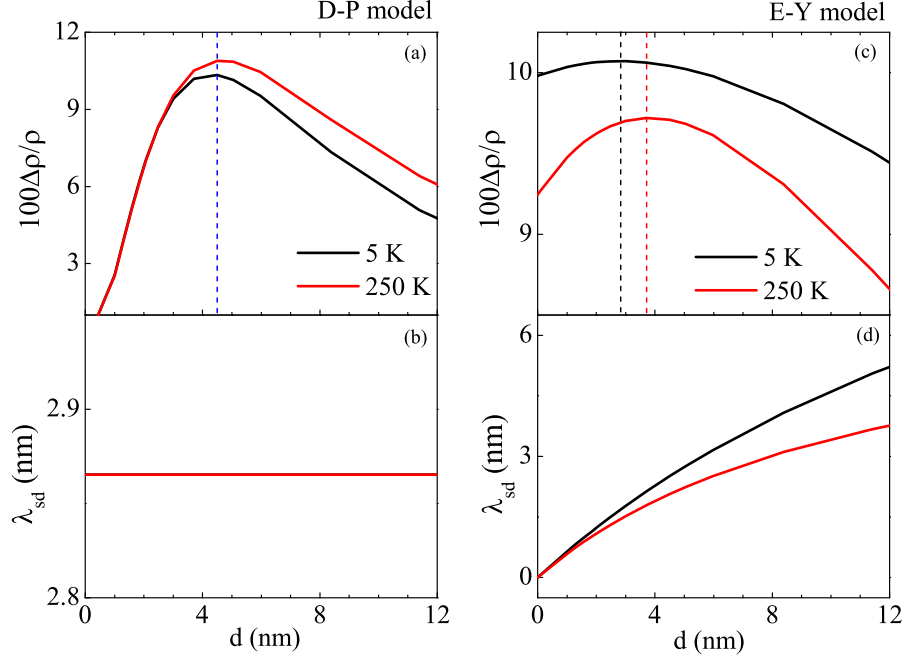


FIG. 6: For Pd/YIG, calculated  $d$  dependencies of the SMR (a, c) and the SDL (b, d) for the D-P (a, b) and the E-Y (c, d) mechanisms. In (a, b, c, d), the SDL  $\lambda_{sd} = \sqrt{D\tau_s}$ . In (a, c), the SMR is calculated from Eq. 4, assuming the SHA  $\theta_{SH} = 1.0$ .  $\tau_s$  in (a, b) and (c, d) is, respectively, calculated by Eqs. 2 and 1, where  $\tau_e = D/v_F^2$ ,  $v_F = \sqrt{2E_F/m}$ ,  $E_F = 7.0$  eV, and  $m$  refers to the mass of free electrons. The parameters  $\alpha = 0$  and  $\langle \Omega_k^2 \rangle = 3 \times 10^{29} \text{ s}^{-2}$  in (a, b), and  $\alpha = 0.1$  and  $\langle \Omega_k^2 \rangle = 0$  in (c, d). The values of  $D$  and  $G_r$  of Pd/YIG were measured, as shown below.

$\mu_H = R_H \sigma$  with the electric conductivity  $\sigma$ , and finally the diffusion coefficient<sup>22</sup>  $D = \frac{E_F \mu_H}{e}$  with  $E_F = 7.0$  eV for Pd. For PdPt/YIG, the SDL is fixed as a function of temperature, as shown in Fig. 7(a). The phonon induced scattering of electron momentum becomes strong at high  $T$  and the relaxation time of electron momentum  $\tau_e$  becomes short. Since  $D \propto \tau_e$ ,  $D$  in Pd (15.0 nm)/YIG is reduced at high  $T$ , as shown in Fig. 7(b). With the data of  $\lambda_{sd}$  and  $D$ , the spin relaxation time  $\tau_s$  in Pd (15.0 nm)/YIG can be evaluated by virtue of  $\lambda_{sd} = \sqrt{D\tau_s}$ , as shown in Fig. 7(c). Since  $1/D$  at a specific temperature, such as 5 K, is a linear function of  $1/d$ ,  $\tau_s$  changes linearly with  $1/d$ , as shown in Figs. 7(d)- 7(e). The interfacial and the bulk spin relaxation times can be clearly separated because  $\tau_s \propto 1/\tau_e$  in the D-P model and the entire electron scattering rate  $1/\tau_e$  is contributed by the interfacial and the bulk ones. The bulk part of  $1/\tau_e$  at 5 K is contributed by defects and impurities in the interior layers. The reduction of the NM thickness results in a shorter  $\tau_e$  and hence prevents the spin flip occurring between two successive collisions. Therefore the total spin relaxation time  $\tau_s$  increases on

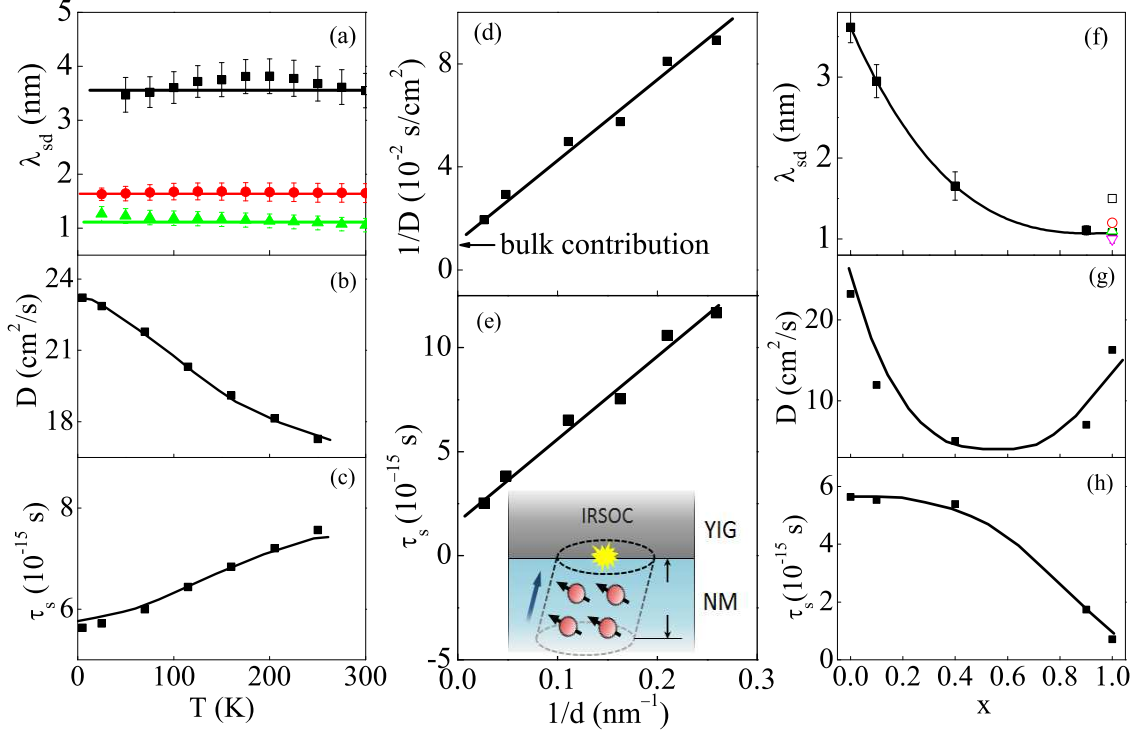


FIG. 7: Temperature dependencies of  $\lambda_{sd}$  (a) in PdPt/YIG with the Pt atomic concentration  $x = 0$  (black solid boxes),  $x = 0.40$  (red solid circles) and  $x = 1.0$  (green solid uptriangle). For Pd/YIG,  $D$  (b) and  $\tau_s$  (c) versus  $T$  at  $d = 15.0$  nm,  $1/D$  (d) and  $\tau_s$  (e) versus  $1/d$  at 5 K. Pt atomic concentration  $x$  dependencies of  $\lambda_{sd}$  (f),  $D$  (g), and  $\tau_s$  (h) at 5 K in PdPt (15.0 nm)/YIG. Solid lines serve a guide to the eye in (b, c, f, g, h) and linear fitting results in (a, d, e). The inset in (e) schematically shows the IRSOC induced spin relaxation process for electrons within the column of the height being the mean free path, i.e.,  $\lambda_e (=v_F\tau_e)$ . In (f), the values of the SDL, taken from other research groups, are given for comparison, including 1.0 nm (open downtriangle)<sup>40</sup>, 1.1 nm (open uptriangle)<sup>14</sup>, 1.2 nm (open circle)<sup>10,19</sup>, 1.5 nm (open box)<sup>13,35,36</sup>. The error bars in (a) and (f) are obtained from the fitting procedure of the NM layer thickness dependencies of the SMR ratio. The R-square is in the region of 0.85-0.97.

decreasing NM layer thickness.

Figure 7(f) shows that  $\lambda_{sd}$  of PdPt(15.0 nm)/YIG, at 5 K, decreases with increasing Pt concentration, where the excitation of phonons is significantly suppressed at low temperatures. The SDL value of the present Pt/YIG agrees with the results of other research groups<sup>10,13,14,19,35,36,40</sup>. The parameter  $D$  reaches a minimum at the intermediate alloy composition, as shown in Fig. 7(g), owing to the random distribution of Pd and Pt atoms. In the E-Y and the D-P models,  $\tau_{s,EY} \propto \xi^{-2}$  and  $\tau_{s,DP} \propto \xi_R^{-2}$ , as shown in Eqs. 1 and 2, thus  $\lambda_{sd} \propto 1/\xi$  and  $1/\xi_R$ , respectively.  $\xi$  and  $\xi_R$  increase with increasing  $x$ , as shown in the appendix, leading to the reduction of  $\lambda_{sd}$  for large  $x$  in the two models. The SDL in the

D-P model is expected to decrease monotonically with increasing  $x$ , in agreement with the results in Fig. 7(f), because it is independent of either  $\tau_e$  or  $D$ . In contrast, with the E-Y model,  $\tau_{s,EY} \propto \tau_e$  and thus  $\lambda_{sd} \propto D$ . The SDL is expected to change *nonmonotonically* with  $x$  after considering the combined effect of the electron momentum scattering and the bulk SOC. Figure 7(h) shows  $\tau_s(\text{Pd})=5.63$  fs,  $\tau_s(\text{Pt})=0.708$  fs, and the ratio  $\tau_s(\text{Pd})/\tau_s(\text{Pt}) = 7.95$ , slightly larger than the theoretical value of 5.78 from Eq. 2, where  $\xi_R(\text{Pd})/\xi_R(\text{Pt}) = 0.364$ , as taken from *ab. initio* calculations in the appendix, and  $\tau_e(\text{Pd})/\tau_e(\text{Pt}) \approx D(\text{Pd})/D(\text{Pt}) = 1.29$ . In quantitative explanations of the SDL behavior, other factors should also be considered. For example, the Fermi surface shape, the Fermi energy, and the effective mass of electrons may change with the Pt concentration<sup>41-43</sup>. Moreover, additional interfacial spin flip scattering, induced by the spin-spin exchange interaction at the magnetic atoms near the interface, should also be taken into account<sup>27</sup>.

Figure 8 summarizes the results of the SHA. It changes nonmonotonically as a function of temperature and the maximum shifts towards high temperatures for high Pt concentrations, as shown in Figs. 8(a)-8(c). The SHA obeys the following scaling law, i.e.,  $\theta_{SH} = a + b\rho$  with  $a$  being the skew scattering parameter and  $b$  being contributed by the side-jump and the intrinsic terms<sup>8</sup>, in a similar way for anomalous Hall effect<sup>44,45</sup>. Gorini *et al.*<sup>46</sup> have theoretically shown that in the presence of IRSOC at the interface between insulator and soft alloy with the Debye temperatures below 300 K, the SHA from the phonon skew scattering,  $a$ , decreases at high temperatures. Meanwhile, the SHA from the linear term, i.e.,  $b\rho$ , increases with increasing temperature<sup>47</sup>. When the extrinsic contributions from the skew scattering and the side-jump at high temperatures are comparable with or smaller than the intrinsic term, the SHA is expected to exhibit a broad maximum as a function of temperature, as shown in Fig. 2 of Ref. 46. The measured nonmonotonic variation of the SHA in Figs. 8(a)- 8(c) eventually verifies the contribution from the phonon skew scattering<sup>46</sup> and the vital effect of the IRSOC, in a good agreement with the D-P spin relaxation process in the present PdPt/YIG. In comparison, the SHA values of Pt/YIG at room temperature are also given from other research groups<sup>14,35,36,38,40,48</sup>.

It is of great interest to address the nonmonotonic variation of the SHA with the Pt concentration  $x$  in Fig. 8(d). At all temperatures, the SHA exhibits a maximum at  $x = 0.90$ . Since the spin relaxation process arises from the interplay between the IRSOC and the scattering of electron momentum, the SHA characteristics are also strongly related to above

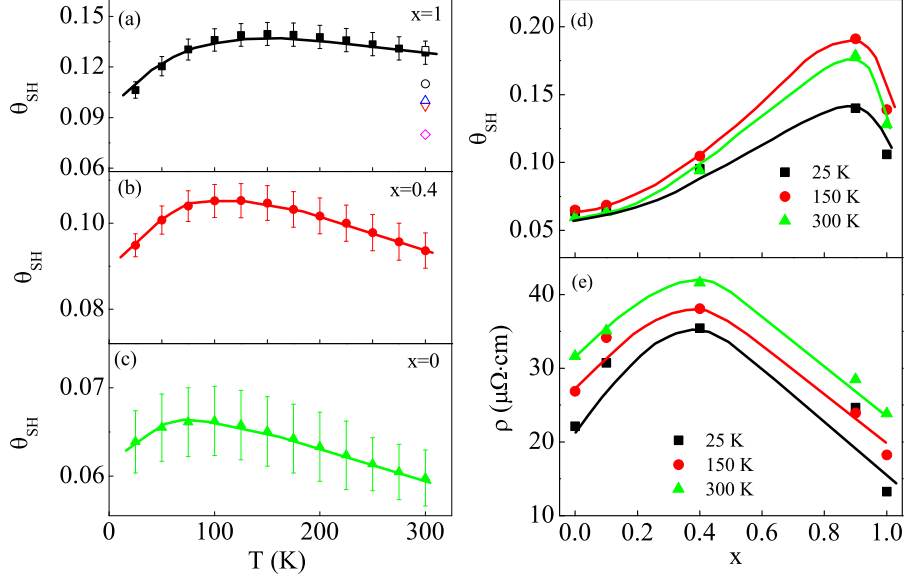


FIG. 8: Temperature dependence of SHA for the Pt concentration  $x = 1.0$  (a),  $0.40$  (b), and  $0$  (c). Dependencies of SHA (d) and  $\rho$  (e) on the Pt concentration. Solid lines serve a guide to the eye. In (a), data taken from other research groups, are given for comparison, including  $0.08$  (open diamond)<sup>14</sup>,  $0.097$  (open downtriangle)<sup>40</sup>,  $0.10$  (open uptriangle)<sup>38</sup>,  $0.11$  (open circle)<sup>13,35,36</sup>,  $0.13$  (open box)<sup>48</sup>. The error bars in (a)-(c) are obtained by the fitting procedure of the NM layer thickness dependencies of the SMR ratio. The R-square is in the region of  $0.85$ - $0.97$ .

two ingredients. In particular, in view of the short SDL, the large SHA in the present PdPt/YIG is dominated by the NM atomic layers near the interface, with a minor contribution from the interior layers<sup>16,47,49,50</sup>. At a specific temperature, the SHA is expected to show a similar variation trend for the sheet resistivity<sup>51,52</sup>, exhibiting a broad maximum at the intermediate alloy composition due to the random distribution of Pt and Pd atoms, as shown in Fig. 8(e). On the other hand, the IRSOC strength  $\xi_R$  increases monotonically with  $x$ , as shown in the appendix, leading to the enhancement of the parameters  $a$  and  $b$ . Because of the combined effect of the IRSOC and the sheet resistivity, the SHA maximum is shifted towards larger  $x$ , compared with that of the sheet resistivity in Fig. 8(e).

The identification of the SDL mechanism allows to solve the big discrepancy in the SDL and the SHA between heterostructures and nonlocal spin valves<sup>6,10,22,40,53,54</sup>. The temperature dependence of the SDL in the present heterostructures is distinctly different from the results in nonlocal spin valves<sup>15,18,40,53</sup>. In the former case, i.e., NM/FM heterostructures, the spin relaxation process is influenced by the D-P model that enabled by the symmetry broken interface and the SDL exhibits weak temperature dependence. In the latter case, the spin

current travels in NM nanowires with a minor effect from the interface, the spin relaxation process obeys the E-Y model, and the SDL exhibits strong temperature dependence<sup>54</sup>. Accordingly, the diversity of the temperature dependence of the SDL in various systems arises from the different spin relaxation mechanisms. Meanwhile, the SHA in Pt/YIG is larger than that of NiFe/Pt/NiFe nonlocal spin valves because for NM/FM heterostructures, the IRSOC adequately contributes to the SHA whereas for nonlocal spin valves, the SHA is dominated by the bulk one<sup>6,10,40,53,54</sup>.

The SDL and the SHA in NM/FM heterostructures can be tuned by the magnitudes of the IRSOC and the scattering rate of the electron momentum which in turn depend on intrinsic physics properties of the NM layer and on the fabrication condition<sup>3</sup>. For example, the SDL is 4.6 nm in Au/YIG<sup>51</sup> and 1.05-3.60 nm in the present PdPt/YIG because most electrons near the Fermi energy are *s* ones with the orbital quantum number  $L = 0$  in Au and *d* ones with  $L = 2$  in PdPt, leading to small and large IRSOC in Au/YIG and PdPt/YIG, respectively. Moreover, for low (high) scattering rate of electron momentum  $1/\tau_e$  and sheet resistivity, the spin relaxation process is mainly dominated by the D-P (E-Y) model, and the SHA is controlled by the interfacial (bulk) physics properties of the NM layer. When the E-Y and the D-P spin relaxation times are comparable at intermediate electron scattering rates, the interfacial and the bulk contributions should both be considered in the SDL and the SHA<sup>22</sup>. For example, the SMR magnitude of Pd/YIG, reported by Lin *et al*<sup>39,47</sup>, is about  $10^{-4}$ , much smaller than the present values of  $10^{-3}$ . Since the IRSOC and the sheet resistivity strongly depend on the interfacial morphology such as the roughness at Pd/YIG interface and the microstructure of the Pd layer, respectively, the big discrepancy can be attributed to different fabrication conditions.

It is significant to compare the results of the SHA and the SDL in the present work to others in literatures. Apparently, the SHA value of the present Pt/YG at room temperature, 0.129, is close to existing experimental values, such as 0.08<sup>14</sup>, 0.097<sup>40</sup>, 0.10<sup>38</sup>, 0.11<sup>13,35,36</sup>, 0.13<sup>48</sup> for Pt/YIG heterostructures, as shown in Fig. 8(a). The value of the SDL, 1.08 nm, is also close to existing experimental values, such as 1.0 nm (open downwards triangle)<sup>40</sup>, 1.1 nm (open upwards triangle)<sup>14</sup>, 1.2 nm (open circles)<sup>10,19</sup>, 1.5 nm (open box)<sup>13,35,36</sup>, as shown in Fig. 7(f). Most of studies have shown the SDL of Pt/YIG falls in the region of 0.5 nm to 1.4 nm<sup>55</sup>. In general, the values of the SHA and the SDL in heterostructures are larger/longer than those of nonlocal systems, highly likely due to other interface effects<sup>55</sup>. In nonlocal systems, the SHA

and the SDL are closer to those of bulk values<sup>56</sup>, where the SHA is as small as 0.02 and the SDL is as long as 5.5-10.0 nm<sup>20,56,57</sup>. In the present work, the interface effects, such as, the spin memory loss and the local distribution of the SHA near the interface, are not considered. These approximations may have a great impact on the fitted values of the SHA and the SDL<sup>16,47,58</sup>. These interface effects should be included in future studies of the relaxation mechanism of the pure spin current. Moreover, in the present work, the SHA is assumed to be independent of the NM layer thickness. The approximation may also have a great impact on the fitting results and the dependence of the SHA on the NM layer thickness should be rigorously studied in the future in order to better understand the relaxation mechanism of the pure spin current.

To summarize, the SDL in PdPt/insulating-YIG is found to be independent of both the temperature and the NM layer thickness, and it decreases monotonically by substituting Pd with heavier Pt atoms. These results indicate the contribution of D-P mechanism in the spin relaxation process due to the IRSOC in NM/FM heterostructures. The nonmonotonic variation of the SHA with temperature is attributed to the combined effect of IRSOC and phonon skew scattering. The temperature-invariance of the SDL and the temperature dependence of the SHA in PdPt/YIG are shown to arise from an identical physics mechanism, i.e., the IRSOC due to the broken symmetry at the NM/FM interface. The present work sheds light on a more comprehensive understanding of spin transport process in NM/FM heterostructures and facilitates the design of the new generation spin orbit torque devices.

### **Acknowledgements**

This work was supported by National Key R & D Program of China Grand No. 2017YFA0305300 and 2017YFA0303202, the State Key Project of Fundamental Research Grant No. 2015CB921501, the National Science Foundation of China Grant Nos. 51331004, 51501131, 51671147, 11874283, 51801152 and 11674246, Natural Science Foundation of Shanghai Grant No. 17ZR1443700, Shanghai Pujiang Program No. 16PJ1409300 and the Program for Professor of Special Appointment (Eastern scholar) at Shanghai Institutions of Higher Learning No. TP2016016, and the Fundamental Research Funds for the Central

Universities.

### **Appendix: *Ab initio* calculation of interfacial Rashba spin orbit coupling in PdPt/YIG**

To quantify the IRSOC strength of PdPt alloys, we performed first-principles calculations using the projected augmented plane-wave method<sup>59,60</sup> as implemented in the Vienna *ab initio* simulation package (VASP)<sup>61</sup>. For brevity of analysis, we constructed a 3-layer slab structure of PdPt alloy, as shown in Fig. 9(a) and the effect of YIG was represented by applying an external electric field (0.1 eV/Å). To eliminate the interaction between supercells, they are separated by a 10 Å vacuum. The exchange correlation of electrons is approximated at the level of the generalized gradient approximation (GGA) in the form of Perdew-Burke-Ernzerhof<sup>62</sup>. SOC is included in the self-consistent calculations. The energy cutoff for the plane-wave expansion was set at 300 eV. We adopted a 25 \* 25 \* 1 k-point grid to sample the two-dimensional Brillouin zone. Atomic relaxation was carried out until the forces were less than less than 0.01 eV/Å.

Since the IRSOC trend obtained in experiments is estimated from the transport measurement where the electrical signal is mainly determined by the states near the Fermi level, we focus on how metallic states behave under the broken inversion symmetry. Degenerated states of two spins start to split when an external electric field is applied as shown in Fig. 9(b). The momentum separation between spin up and down states is proportional to the strength of IRSOC in accordance with the Rashba Hamiltonian<sup>63</sup>. Therefore, the integration of spin splitting for all states that cross the Fermi level is a convincing criterion for the quantification of the IRSOC in PdPt alloys. For a certain Pt concentration ( $x$ ), we defined momentum splitting ( $\Delta k_{Fx}$ ) which is given as where  $i$  is the state index and  $k$  is the Fermi momentum [Fig. 9(c), inset]. To compare the IRSOC strengths of PdPt alloys, we plotted normalized momentum splitting ( $\Delta k_{Fx}/\Delta k_{F0}$ ) as a function of Pt concentration [Fig. 9(c)]. As a result, we found the similar trend of the IRSOC as estimated from the experimental data in Fig. 7(f) and Fig. 8(d). Therefore, we can conclude that the IRSOC is enhanced by the increase of Pt concentration in PdPt alloys. Moreover, the bulk SOC in PdPt alloys also increases with increasing  $x$ , as shown in Fig. 10<sup>37</sup>. Note that other factors such as the induced magnetization in Pd/Pt atoms and the Pt(Pd)-YIG hybridization are not included in the present study. Furthermore, we used only symmetric models with alternating Pt/Pd layers so as to eliminate the artificial Rashba

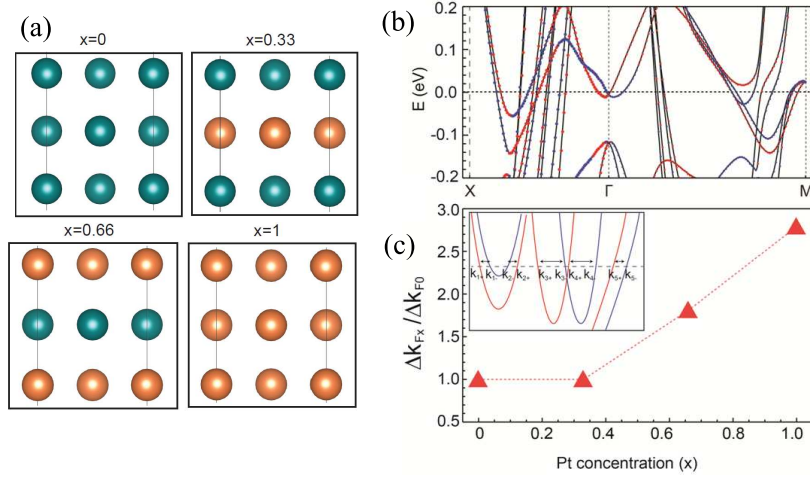


FIG. 9: (a) Schematic pictures of 3-layer slab structure of PdPt alloy. (b) Calculated band structure of Pt thin film when  $0.1 \text{ eV/\AA}$  of electric field is applied. Spin up (down) states are marked by red (blue) dots. (c) The variation of normalized momentum splitting in PdPt with Pt concentration  $x$ .  $\Delta k_{Fx}$  represents the summation of momentum splitting between spin up and down states at the Fermi level for a certain Pt concentration  $x$ . Inset in (c) is a schematic band structure of PdPt alloys. The momentum separation is produced by the IRSOC at the Fermi level. Spin up (down) states are denoted by +(-).

SOC due to structural asymmetry. Therefore, the results of the DFT calculations should be viewed as qualitative explanations of our observations. Nonetheless, the good agreement in trend suggests that the driving force of IRSOC is the electric field on the YIG surface.

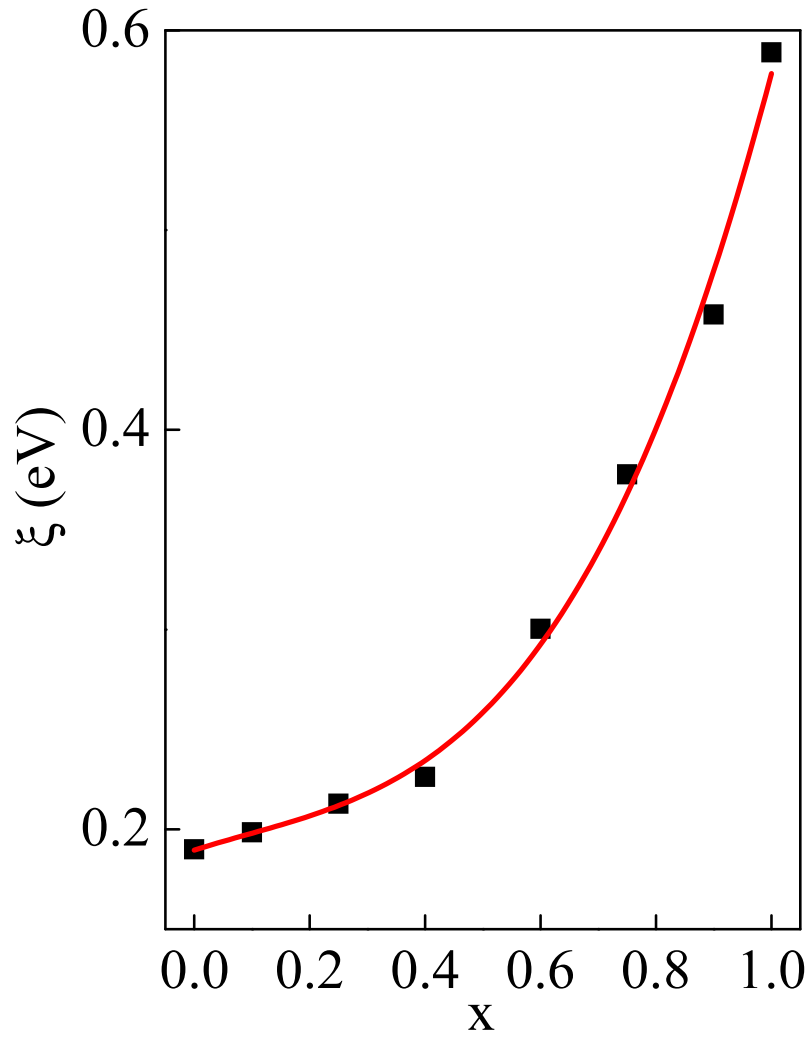


FIG. 10: The bulk SOC in PdPt versus the Pt concentration  $x$ . Here the data were taken from Ref. 37.

- 
- \* Electronic address: [xpqiu@tongji.edu.cn](mailto:xpqiu@tongji.edu.cn)
- <sup>1</sup> I. M. Miron, K. Garello, G. Gaudin, P. J. Zermatten, M. V. Costache, S. Auffret, S. Bandiera, B. Rodmacq, A. Schuhl, and P. Gambardella, *Nature* **476**, 189 (2011)
  - <sup>2</sup> L. Liu, O. Lee, T. Gudmundsen, D. Ralph and R. Buhrman, *Phys. Rev. Lett.* **109**, 096602 (2012)
  - <sup>3</sup> X. Qiu, K. Narayanapillai, Y. Wu, P. Deorani, D.-H. Yang, W.-S. Noh, J.-H. Park, K.-J. Lee, H.-W. Lee, and H. Yang, *Nat. Nanotechnol.* **10**, 333 (2015)
  - <sup>4</sup> A. Fert, V. Cros and J. Sampaio, *Nat. Nanotechnol.* **8**, 152 (2013)
  - <sup>5</sup> T. J. Huisman, R. V. Mikhaylovskiy, J. D. Costa, F. Freimuth, E. Paz, J. Ventura, P. P. Freitas, S. Blgel, Y. Mokrousov, T. Rasing, and A. V. Kimel, *Nat. Nanotechnol.* **11**, 455 (2016)
  - <sup>6</sup> H. Nakayama, M. Althammer, Y. T. Chen, K. Uchida, Y. Kajiwara, D. Kikuchi, T. Ohtani, S. Geprägs, M. Opel, S. Takahashi, R. Gross, G. E. W. Bauer, S. T. B. Goennenwein, and E. Saitoh, *Phys. Rev. Lett.* **110**, 206601 (2013)
  - <sup>7</sup> I. Žutió, J. Fabian, and S. Das Sarma, *Rev. Mod. Phys.* **76**, 323 (2004)
  - <sup>8</sup> S. Takahashi and S. Maekawa, *Sci. Technol. Adv. Mater.* **9**, 014105 (2008)
  - <sup>9</sup> J. Sinova, S. O. Valenzuela, J. Wunderlich, C. H. Back, and T. Jungwirth, *Rev. Mod. Phys.* **87**, 1213 (2015)
  - <sup>10</sup> W. Zhang, V. Vlaminck, J.E. Pearson, R. Divan, S. D. Bader, and A. Hoffmann, *Appl. Phys. Lett.* **103**, 242414 (2013)
  - <sup>11</sup> M. Costache, M. Sladkov, S. Watts, C. van der Wal, and B. van Wees, *Phys. Rev. Lett.* **97**, 216603(2006)
  - <sup>12</sup> F. D. Czeschka, L. Dreher, M. S. Brandt, M. Weiler, M. Althammer, I. M. Imort, G. Reiss, A. Thomas, W. Schoch, W. Limmer, H. Huebl, R. Gross, and S. T. B. Goennenwein, *Phys. Rev. Lett.* **107**, 046601 (2011)
  - <sup>13</sup> M. Althammer, S. Meyer, H. Nakayama, M. Schreier, S. Altmannshofer, M. Weiler, H. Huebl, S. Geprägs, M. Opel, R. Gross, D. Meier, C. Klewe, T. Kuschel, J.-M. Schmalhorst, G. Reiss, L. Shen, A. Gupta, Y.-T. Chen, G. E. W. Bauer, E. Saitoh, and S. T. B. Goennenwein, *Phys. Rev. B* **87**, 224401 (2013)
  - <sup>14</sup> N. Vlietstra, J. Shan, V. Castel, J. Ben Youssef, G. E. W. Bauer, and B. J. van Wees, *Appl. Phys. Lett.* **103**, 032401 (2013)

- <sup>15</sup> Y. Liu, Z. Yuan, R. J. H. Wesselink, A. A. Starikov, M. van Schilfgaarde, and P. J. Kelly, Phys. Rev. B **91**, 220405(R) (2015)
- <sup>16</sup> K. Chen and S. Zhang, Phys. Rev. Lett. **114**, 126602 (2015)
- <sup>17</sup> M. H. Nguyen, D. C. Ralph, and R. A. Buhrman, Phys. Rev. Lett. **116**, 126601 (2016)
- <sup>18</sup> S. R. Marmion, M. Ali, M. McLaren, D. A. Williams, and B. J. Hickey, Phys. Rev. B **89**, 220404(R) (2014)
- <sup>19</sup> S. Meyer, M. Althammer, S. Geprägs, M. Opel, R. Gross, and S. T. B. Goennenwein, Appl. Phys. Lett. **104**, 242411 (2014)
- <sup>20</sup> Y. Liu, Z. Yuan, R. J. H. Wesselink, A. A. Starikov, and P. J. Kelly, Phys. Rev. Lett. **113**, 207202 (2014)
- <sup>21</sup> C. T. Boone, J. M. Shaw, H. T. Nembach, and T. J. Silva, J. Appl. Phys. **117**, 223910 (2015)
- <sup>22</sup> J. Ryu, M. Kohda, and J. Nitta, Phys. Rev. Lett. **116**, 256802 (2016)
- <sup>23</sup> H. Emoto, Y. Ando, G. Eguchi, R. Ohshima, E. Shikoh, Y. Fuseya, T. Shinjo and M. Shiraishi, Phys. Rev. B **93**, 174428 (2016)
- <sup>24</sup> R. J. Elliott, Phys. Rev. **96**, 266 (1954)
- <sup>25</sup> Y. Yafet, J. Phys. Chem. Solids **21**, 99 (1961)
- <sup>26</sup> Y. Yafet, in *Solid State Physics*, Vol. **14**, edited by F. Seitz and D. Turnbull (Academic, New York, 1963), pp.1-98
- <sup>27</sup> J. Fabian and S. Das Sarma, J. Vac. Sci. Tech. B **17**, 1708 (1999)
- <sup>28</sup> M. Dyakonov and V. Perel, Sov. Phys. Solid State **13**, 3023 (1972)
- <sup>29</sup> M. D. Mower, G. Vignale, and I. V. Tokatly, Phys. Rev. B **83**, 155205 (2011)
- <sup>30</sup> N. H. Long, P. Mavropoulos, D. S. G. Bauer, B. Zimmermann, Y. Mokrousov and S. Blugel, Phys. Rev. B **94**, 180406(R) (2016)
- <sup>31</sup> R. Freeman, A. Zholud, Z. Dun, H. Zhou and S. Urazhdin, Phys. Rev. Lett. **120**, 067204 (2018)
- <sup>32</sup> A. Manchon, H.C. Koo, J. Nitta, S. M. Frolov, and R. A. Duine, Nat. Mater. **14**, 871 (2015)
- <sup>33</sup> T. Valet and A. Fert, Phys. Rev. B **48**, 7099 (1993)
- <sup>34</sup> L. R. Windmiller, J. B. Ketterson, and S. Hornfeldt, J. Appl. Phys. **40**, 1291 (1969)
- <sup>35</sup> M. Haertinger, C. H. Back, J. Lotze, M. Weiler, S. Geprägs, H. Huebl, S. T. B. Goennenwein, and G. Woltersdorf, Phys. Rev. B **92**, 054437(2015)
- <sup>36</sup> M. Weiler, M. Althammer, M. Schreier, J. Lotze, M. Pernpeintner, S. Meyer, H. Huebl, R. Gross, A. Kamra, J. Xiao, Y. T. Chen, H. Jiao, G. E. W. Bauer, and S. T. B. Goennenwein, Phys. Rev.

- Lett. **111**, 176601(2013)
- <sup>37</sup> L. Ma, H. A. Zhou, L. Wang, X. L. Fan, W. J. Fan, D. S. Xue, K. Xia, Z. Wang, R. Q. Wu, G. Y. Guo, L. Sun, X. Wang, X. M. Cheng, and S. M. Zhou, *Adv. Electron. Mater.* **2**, 1600112 (2016)
- <sup>38</sup> H. L. Wang, C. H. Du, Y. Pu, R. Adur, P. C. Hammel, F. Y. Yang, *Phys. Rev. Lett.* **112**, 197201(2014)
- <sup>39</sup> T. Lin, C. Tang, H. M. Alyahyaei, and J. Shi, *Phys. Rev. Lett.* **113**, 037203 (2014)
- <sup>40</sup> M. Morota, Y. Niimi, K. Ohnishi, D. H. Wei, T. Tanaka, H. Kontani, T. Kimura, and Y. Otani, *Phys. Rev. B* **83**, 174405 (2011)
- <sup>41</sup> O. K. Andersen and A. R. Mackintosh, *Solid State Commun.* **6**, 285 (1968)
- <sup>42</sup> O. K. Andersen, *Phys. Rev. B* **2**, 883 (1970)
- <sup>43</sup> X. Zhou, L. Ma, Z. Shi, G. Y. Guo, J. Hu, R. Q. Wu, and S. M. Zhou, *Appl. Phys. Lett.* **105**, 012408 (2014)
- <sup>44</sup> P. He, L. Ma, Z. Shi, G.Y. Guo, J.-G. Zheng, Y. Xin, and S. M. Zhou, *Phys. Rev. Lett.* **109**, 066402 (2012)
- <sup>45</sup> Y. Tian, L. Ye, and X. F. Jin, *Phys. Rev. Lett.* **103**, 087206 (2009)
- <sup>46</sup> C. Gorini, U. Eckern, and R. Raimondi, *Phys. Rev. Lett.* **115**, 076602 (2015)
- <sup>47</sup> L. Wang, R. J. H. Wesselink, Y. Liu, Z. Yuan, K. Xia and P. J. Kelly, *Phys. Rev. Lett.* **116**, 196602 (2016)
- <sup>48</sup> D. Qu, S. Y. Huang, B. F. Miao, S. X. Huang, and C. L. Chien, *Phys. Rev. B* **89**, 140407(2014)
- <sup>49</sup> V. P. Amin and M. D. Stiles, *Phys. Rev. B* **94**, 104420 (2016)
- <sup>50</sup> F. Freimuth, S. Blügel, and Y. Mokrousov, *Phys. Rev. B* **92**, 064415 (2015)
- <sup>51</sup> L. K. Zou, S. H. Wang, Y. Zhang, J. R. Sun, J. W. Cai, and S. S. Kang, *Phys. Rev. B* **93**, 014422 (2016)
- <sup>52</sup> M. Obstbaum, M. Decker, A. K. Greitner, M. Haertinger, T. N. G. Meier, M. Kronseder, K. Chadova, S. Wimmer, D. Ködderitzsch, H. Ebert, and C. H. Back, *Phys. Rev. Lett.* **117**, 167204 (2016)
- <sup>53</sup> L. Q. Liu, R. A. Buhrman, and D. C. Ralph, arXiv: 1111.3702 (2011)
- <sup>54</sup> M. Isasa, E. Villamor, L. E. Hueso, M. Gradhand, and F. Casanova, *Phys. Rev. B* **91**, 024402 (2015)
- <sup>55</sup> *see*, Table III, *in* J. Sinova, S. O. Valenzuela, J. Wunderlich, C. H. Back, T. Jungwirth, *Rev. Mod. Phys.* **87**, 1213(2015)

- <sup>56</sup> *see*, Table I, *in* Y. Niimi and Y. Otani, Rep. Prog. Phys. **78**, 124501(2015)
- <sup>57</sup> A. A. Starikov, P. J. Kelly, A. Brataas, Y. Tserkovnyak, and G. E. W. Bauer, Phys. Rev. Lett. **105**, 236601(2010)
- <sup>58</sup> X. D. Tao, Q. Liu, B. F. Miao, R. Yu, Z. Feng, L. Sun, B. You, J. Du, K. Chen, S. F. Zhang, L. Zhang, Z. Yuan, D. Wu, and H. F. Ding, Sci. Adv. **4**, eaat1670(2018)
- <sup>59</sup> P. E. Blöchl, Phys. Rev. B **50**, 17953 (1994)
- <sup>60</sup> G. Kresse, and D. Joubert, Phys. Rev. B **59**, 1758 (1999)
- <sup>61</sup> G. Kresse, and J. Hafner, Phys. Rev. B **49**, 14251 (1994)
- <sup>62</sup> J. P. Perdew, K. Burke, and M. Ernzerhof, Phys. Rev. Lett. **77**, 3865 (1996)
- <sup>63</sup> S. Grytsyuk, A. Belabbes, P. M. Haney, H.-W. Lee, K.-J. Lee, M. D. Stiles, U. Schwingenschlögl, and A. Manchon, Phys. Rev. B **93**, 174421(2016)